



Hydration of salts as a two-step process: Water adsorption and hydrate formation

Leyla-Cann Sögütöglü^a, Felix Birkelbach^b, Andreas Werner^b, Hartmut Fischer^c,
Henk Huinink^{a,*}, Olaf Adan^{a,c}

^a Technical University Eindhoven, P.O. Box 513, Department of Applied Physics, 5600 MB Eindhoven, The Netherlands

^b TU Wien, Institute for Energy Systems and Thermodynamics, Getreidemarkt 9/E302, 1060 Vienna, Austria

^c Netherlands Organization for Applied Scientific Research (TNO), High Tech Campus 25, 5656 AE Eindhoven, The Netherlands

ARTICLE INFO

Keywords:

Hydration of salts
K₂CO₃
Thermochemical energy storage
Non-parametric kinetic analysis
Nucleation

ABSTRACT

K₂CO₃ is a promising salt for thermochemical heat storage. For a high performance, the thermochemical reaction must take place as close as possible to the equilibrium, while ensuring sufficient reaction rates. In this work, we studied the near-equilibrium hydration kinetics of K₂CO₃ and other salts (CuCl₂, MgCl₂ and LiCl). We proposed a generic two-step mechanism for the hydration of salts, consisting of (1) adsorption of water vapour and dissolution of ions from the initial phase (a wetting film) and (2) formation of the hydrate crystal (crystallisation from the wetting film). The two steps are assumed to be in momentary balance during the hydration process. As a result, nucleation is rate limiting at low supersaturations of water vapour (inside the metastable zone), and water diffusion to the wetting film is rate limiting at high supersaturations (outside the metastable zone). We have seen that the vapour pressure of the wetting film stabilises at the metastable zone boundary p^* . The driving force for hydration outside the metastable zone (MZ) is therefore the pressure difference between the atmospheric vapour pressure and the vapour pressure of the wetting film, $p - p^*$. Non-Parametric Kinetic analysis of the hydration of K₂CO₃ indicates that nucleation plays a central role inside the metastable zone (at low supersaturations) as expected. Outside the MZ, the analysis suggests a steady conversion rate, in agreement with a water vapour diffusion limitation. The diffusion limited process at high supersaturations hardly depends on the temperature, but mainly on the pressure difference, as expected. It is further shown that the diffusion limited process can be characterised with an apparent activation energy. However, this apparent activation energy is in fact the hydration enthalpy and does not refer to a real energy barrier.

1. Introduction

Thermochemical heat storage is a proven concept for compact domestic heat storage and is based on the reversible reaction of the solid thermochemical material and a gas. Heat can be stored virtually loss-free in the absence of the gas and can be extracted at domestic usage temperatures, typically between 30–70 °C [1,2].

Recently, K₂CO₃ was identified as one of the most promising salt hydrates for thermochemical heat storage [3]. The compound is chemically and physically robust compared to other candidates which have been studied in detail such as MgCl₂ [4–7], CaCl₂ [8,9], MgSO₄ [10,11] and Na₂S [12,13,7]. The latter compounds, in contrast to K₂CO₃, lose their heat storage capacity due to chemical degradation (MgCl₂, Na₂S [7]) or due to clogging (MgCl₂, CaCl₂, MgSO₄). Mitigation routes are

therefore necessary and have been studied extensively [14,15].

K₂CO₃ has an energy density of 1.28 GJ/m³ when fully dehydrated by heating to 100 °C. Based on cyclic measurements, the compound can store 15–66 GJ annually, repeated over at least 20 years [7]. The salt has a reversible reaction from anhydrous to sesquihydrate:



where the anhydrous phase is referred to as α and the sesquihydrate is referred to as β . The reaction is in equilibrium at 59 °C at a partial water vapour pressure p of 12 mbar. That means that the material could deliver a temperature of 59 °C when exposed to water vapour of 12 mbar (a typical water vapour in winter in Western Europe, i.e., a water source of 10 °C [3]).

However, the reaction rate is inhibited above 45 °C, which is 14 °C below the equilibrium temperature [16,17]. As a consequence, the

* Corresponding author.

E-mail address: h.p.huinink@tue.nl (H. Huinink).

<https://doi.org/10.1016/j.tca.2020.178819>

Received 21 May 2020; Received in revised form 19 October 2020; Accepted 21 November 2020

Available online 26 November 2020

0040-6031/© 2020 The Author(s). Published by Elsevier B.V. This is an open access article under the CC BY license (<http://creativecommons.org/licenses/by/4.0/>).

Nomenclature*Acronyms*

DSC	differential scanning calorimetry
MZB	metastable zone boundary
MZ	metastable zone
TCES	thermochemical energy storage
TES	thermal energy storage
TGA	thermogravimetric analysis
SDTA	simultaneous differential thermal analysis

Greek symbols

α	conversion
$d\alpha/dt$	reaction rate, 1/s
ΔH^0	hydration enthalpy per mole water, J/mol
ΔS^0	hydration entropy per mole water, J/mol K
$\Delta\mu$	difference in chemical potential, J/mol
μ	chemical potential of water, J/mol

Roman symbols

a, b	stoichiometric coefficients
D	diffusion constant, m^2 1/s
d	boundary layer thickness, m
ΔG	Gibbs free energy of hydration per mole water, J/mol
$f(\alpha)$	conversion dependency, reaction model
J	molar flux, mol/ m^2 s
J_{nuc}	nucleation rate, 1/s
$h(\dots)$	driving force dependency
$k(T)$	temperature dependency, 1/s
p^0	reference pressure, 10^5 Pa
p	partial pressure of gas, Pa
p^*	partial pressure at metastable zone boundary, Pa
p_{eq}	equilibrium partial pressure of gas, Pa
p_f	partial pressure at the film, Pa
R	universal gas constant, J/mol K
T	temperature, K
t	time, s

maximum temperature at which heat can be extracted under working conditions is 45 °C with a peak power of 130 W/kg at 33 °C [3,7].

The performance of a thermochemical material is defined by temperature and reaction rate. The temperature at which heat can be extracted is limited by the reaction equilibrium. For a high performance, the storage must be operated as close as possible to the equilibrium, while ensuring sufficient reaction rates. Thus, knowledge of the reaction kinetics in close vicinity of the equilibrium is required to design an efficient heat battery.

Also for other salts, the conversion rate was found to be inhibited at vapour pressures close to equilibrium [17–19]. Recently, the near-equilibrium zone was framed as a metastable zone (MZ) where nucleation and growth processes play a role. It was hypothesised that the hydration proceeds through a wetting layer, that is, a mobile wetting film with water and ions from which the new phase can crystallise [17].

In this work, a generic hydration mechanism is proposed for salts, based on which we formulate the rate-limiting step in the hydration process. We evaluate our hypothesis using an independent tool, non-parametric kinetic analysis, as described by Birkelbach [20]. Two different driving forces are considered in order to test our assumptions about the rate-limiting step in the hydration process.

2. Materials and methods

$K_2CO_3 \cdot 1.5H_2O$ (pro analysis) was purchased from Sigma-Aldrich. $CuCl_2 \cdot 2H_2O$, $MgCl_2 \cdot 6H_2O$ and $LiCl$ (pro analysis) were purchased from Merck. All salts were sieved to 50–164 μm size fraction, which is the typical powder size used to compact K_2CO_3 in the form of granules for thermochemical heat storage application. The salts were sieved to the same size for experimental comparison and were used without any further purification.

A thermogravimetric analyser of type Mettler-Toledo TGA/SDTA 851e was equipped with a home-built humidity generator. Humidified nitrogen was used as reactive gas (500 mL/min). The reactive gas was brought to the desired water vapour pressure by mixing dry gas (0% RH) and wet gas (100% RH) at a controlled temperature of 21 °C. The water vapour pressure was calibrated with an accuracy of ± 0.5 mbar using the gravimetric signal at the deliquescence point of $LiCl \cdot H_2O$, CH_3COOK , $K_2CO_3 \cdot 1.5H_2O$, $MgCl_2 \cdot 6H_2O$ and $Mg(NO_3)_2 \cdot 6H_2O$ at 25 °C and $LiCl \cdot H_2O$ at 40; 50; 55; 60 °C [21]. Temperature calibration was performed using the Simultaneous Differential Thermal Analysis (SDTA)-signal of melting points of Indium, Zinc and Aluminium. In case of an endothermic process such as melting, a differential signal is observed [22].

Approximately 5 mg of the hydrated salt was placed in a 40 μL

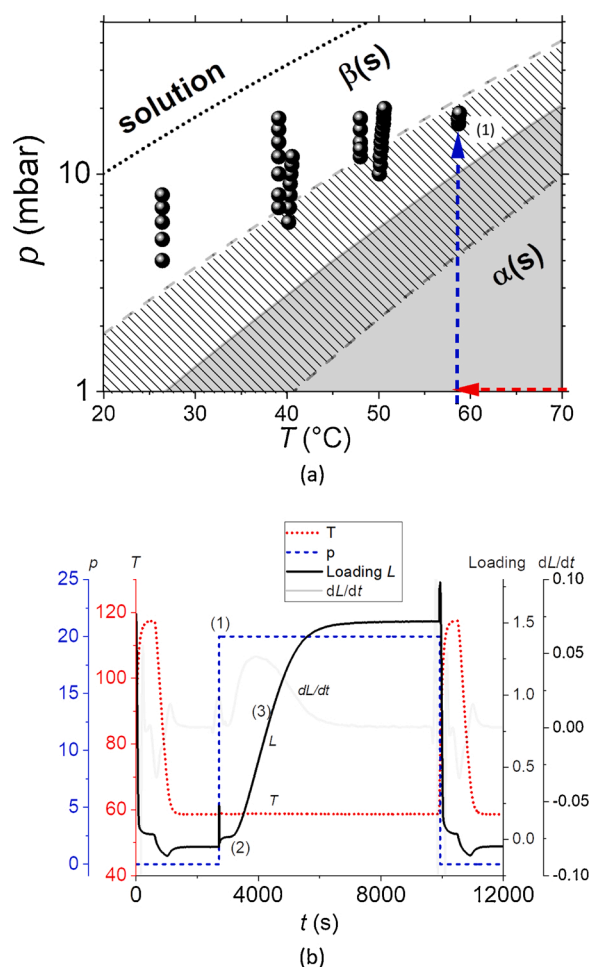


Fig. 1. (a) p - T -phase diagram of K_2CO_3 indicating the experimental conditions (indicated by the bullets) in isothermal-isobaric experiments. The metastable zone is hatched. (b) Example of a hydration experiment, conditions shown by the arrows in (a). The sample dehydrated at $T = 115$ °C and $p = 0$ mbar. Afterwards, the temperature is changed to $T = 58$ °C. Next, the pressure is adapted to $p = 20$ mbar – point (1) – to induce hydration. The hydration onset (2) and maximum rate of conversion (3) are indicated.

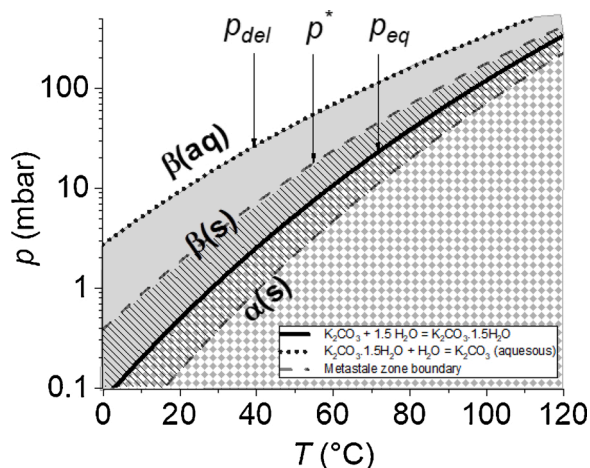


Fig. 2. Experimental phase diagram of K_2CO_3 . The following transition lines are indicated: deliquescence pressure of $K_2CO_3 \cdot 1.5H_2O$ p_{del} (dotted line); metastable zone boundary p^* (dashed lines); hydration equilibrium pressure p_{eq} (solid line). The region where $K_2CO_3 \cdot 1.5H_2O$ is stable is shown in solid grey. The region where K_2CO_3 is stable is hatched.

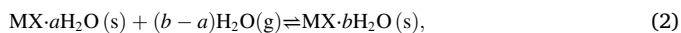
Mettler-Toledo standard aluminium pan without lid. As reproducibility check, isothermal-isobaric hydration experiments were performed twice on $K_2CO_3 \cdot 1.5H_2O$. The experiment was performed at the following temperatures: $T = 40, 50$ and 58 °C (experiment 1) and $T = 25, 40$ and 50 °C (experiment 2) at vapour pressures between 4–20 mbar.

A typical hydration experiment is shown in Fig. 1. The p - T -conditions of the experiments are indicated by the bullets in the phase diagram in Fig. 1a. The sample was prepared in anhydrous phase (K_2CO_3) by drying at $p = 0$ mbar and $T = 115$ °C. After the drying step, the temperature is changed to the hydration temperature, $T = 58$ °C. When the temperature is stable at 58 °C, the hydration pressure (20 mbar) is applied to start hydration. Fig. 1b shows that a relatively short induction period passes after applying the hydration pressure, point (1). Hydration starts at point (2) and the hydration rate typically reaches a maximum after half conversion, point (3). For further details, we refer to the Data in Brief.

3. Current view on the hydration process

3.1. Phase behaviour of salt hydrates

The hydration of a salt involves a complex solid-solid phase transition, where the starting lattice of the α -phase reorganises to the more stable lattice of the β -phase by incorporation of fluid water. The generic equilibrium reaction is



where $MX \cdot aH_2O$ represents the lower hydrated phase α , $MX \cdot bH_2O$ represents the higher hydrated phase β and $(b - a)$ is the stoichiometric coefficient of the water.

From a thermodynamic perspective this reaction is characterised in standard conditions by the reaction Gibbs free energy ΔG^0 [J/mol]

$$\Delta G^0 = \Delta H^0 - T\Delta S^0 = RT \ln \frac{p_{eq}}{p^0}, \quad (3)$$

where ΔH^0 [J/mol] is the reaction enthalpy per mole water at standard conditions, T [K] is the absolute temperature, ΔS^0 [J/mol K] is the reaction entropy per mole water at standard conditions, R [J/mol K] is the gas constant, p_{eq} [Pa] is the partial pressure of vapour in equilibrium with the salt and $p^0 = 10^5$ Pa is the standard pressure.

The water vapour pressure at which the gaseous phase and the condensed phase are in equilibrium, p_{eq} [Pa], is then described by the following thermodynamic relation:

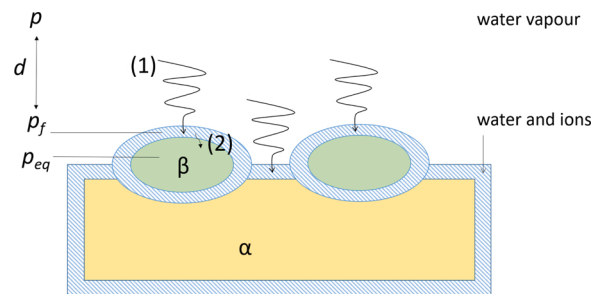


Fig. 3. Schematic cartoon illustrating the two-step hydration process. (1) Adsorption of water and dissolution of ions from the original phase α . (2) Formation of the new crystalline hydrated phase β . p is the partial pressure of the water vapour in the atmosphere, p_f is the vapour pressure of water in equilibrium with the wetting film (hatched) and p_{eq} is the vapour pressure of water in equilibrium with the hydrate. The boundary layer thickness between atmosphere and wetting film is indicated with d .

$$p_{eq} = p^0 \exp(-\Delta S^0/R) \exp(\Delta H^0/RT). \quad (4)$$

There is a thermodynamic driving force for hydration if $p > p_{eq}$. I.e., when $p > p_{eq}$, the β phase is thermodynamically more stable than the α phase. Water will be taken up by the salt and β will be formed. At $p < p_{eq}$ the opposite holds. The phase behaviour of K_2CO_3 is given in the phase diagram in Fig. 2 [17]. The β -phase is stable until it dissolves as a result of a second transition, called deliquescence. At the deliquescence point, p_{del} , the β -phase forms an aqueous solution by further water uptake.

Reaction (2) does not always start instantaneously at water vapour pressures $p > p_{eq}$. This is because the initial formation of the new phase can form a barrier for the hydration transition [17]. The initial stage of a phase transition, in which small nuclei of the new phase are formed is called *nucleation*. If nucleation proceeds very slowly, the old phase is said to be metastable. The upper dashed line (the metastable zone boundary) in Fig. 2 marks the limit of the metastable zone: above that line, the α -phase is unstable. The metastable zone boundary (MZB) is indicated by p^* . Note that the β -phase is also metastable (lower dashed line).

3.2. The proposed mechanism of hydration

Building on the current view of hydration and water-salt interaction [17,18,23], here we hypothesise the mechanism of hydration as a two-step process. The hypothesis is schematically illustrated in Fig. 3. The hydration process is viewed in total, i.e., the travel of a water molecule from the atmosphere to its final position in the lattice. We can cluster the travel in two steps: Step (1) – adsorption to the surface from atmosphere and Step (2) – inclusion from the surface into the final lattice position.

In step (1) sub-processes occur such as diffusion from atmosphere to wetting layer; adsorption of water; mobilisation/dissolution of ions; exclusion of water from the initial phase. In step (2) inclusion of water into the final phase and formation of the crystalline structure (crystallisation) will play a role.

The cartoon in Fig. 3 is simplified in the sense that it suggests nuclei of the crystalline β phase in a wetting layer. However, it is more likely that there is no real α and β phase in proximity of the mobile wetting film, but rather a disordered cluster of ions and water, resembling the final crystalline β phase.

The basic driving force for process (1), adsorption onto the wetting layer, is the difference between the chemical potential of water vapour in the air μ and the chemical potential of water vapour in equilibrium with the wetting film μ_f . Since the chemical potential can be described in terms of the vapour pressure p at low vapour pressures

$$\Delta\mu_{(1)} = \mu - \mu_f = RT \ln(p/p_f), \quad (5)$$

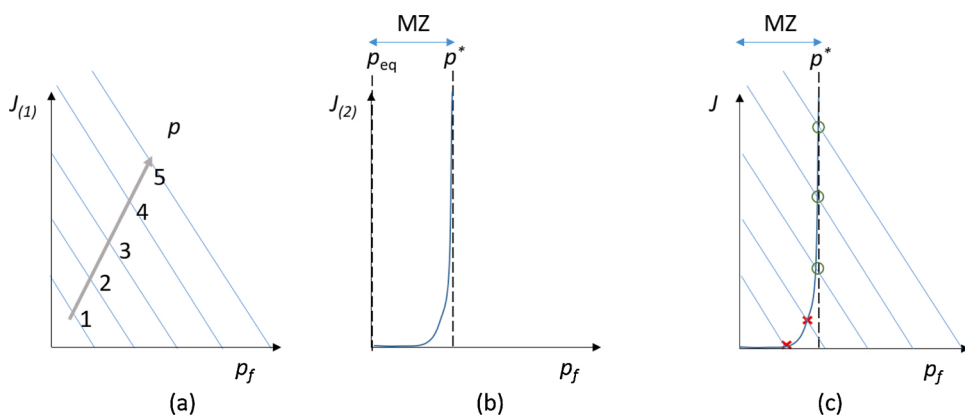


Fig. 4. (a) The adsorption rate $J_{(1)}$ as a function of the film vapour pressure p_f . (b) The hydrate formation rate $J_{(2)}$ as a function of the film vapour pressure p_f . (c) Steady-state situation where intersections represent adsorption of water molecules in balance with incorporation of water molecules. In the metastable zone (MZ), the conversion rate is dictated by the nucleation rate (intersections indicated with crosses). Above the metastable zone boundary (p^*), the conversion rate is dictated by the adsorption rate (intersections indicated with circles).

where p and p_f are the partial pressures of water vapour in the air and of water vapour in equilibrium with the wetting film respectively.

The driving force for process (2), incorporation of water from wetting film into the hydrate crystal, is the difference between the chemical potential of water vapour in equilibrium with the wetting film μ_f and the chemical potential of water vapour in equilibrium with the hydrate μ_{eq} ,

$$\Delta\mu_{(2)} = \mu_f - \mu_{eq} = RT \ln(p_f/p_{eq}), \quad (6)$$

where p_{eq} is the partial pressure of water vapour in equilibrium with hydrate crystal.

We will address the rate of the two processes in terms of the vapour pressure of the film, p_f . After that, we will discuss the rate limiting step based on the steady-state approximation. The two-step mechanism is expected in general, disregarding the crystallite size or shape, because the fundamental phenomena of surface wetting and nucleation of the new phase hold for any type of crystallite.

For the rate of water adsorption onto the film, we first consider the mean-free-path of a gas molecule in atmospheric pressures (tens of nanometers) [24]. The stagnant air layer d at the particle surface will be much thicker than the mean-free-path and therefore Fick's law is a decent approach to express the rate of water adsorption. Here, we

assume that the water directly deposits in the wetting layer once it has reached it. I.e., no specific binding sites or grade of surface coverage is assumed. Fick's law followed by using the gradient of the chemical potential of water vapour $\frac{\partial\mu}{\partial x}$ with $0 < x < d$:

$$J_{(1)} = \frac{D}{dRT}(p - p_f), \quad (7)$$

where, D [m^2/s] is the diffusion constant and d [m] is the boundary layer thickness. The resulting rate dependency as a function of p_f is schematically plotted in Fig. 4a. At $p = p_f$, the adsorption rate is zero. This is illustrated for five different pressures p , from low (1) to high (5) vapour pressure p .

The rate of water incorporation as a function of p_f is shown in Fig. 4b. Earlier work indicates that this rate is subjected to a nucleation barrier [17] as a result of favourable bulk and disfavoured surface contributions of the nucleus. Therefore, the pressure dependency of the rate is described by the nucleation rate:

$$J_{(2)} = \frac{\kappa}{c} \exp\left(\frac{-\lambda}{\ln^2 p_f/p_{eq}}\right), \quad (8)$$

with κ [s^{-1}] a kinetic parameter, λ [-] a thermodynamic parameter, and

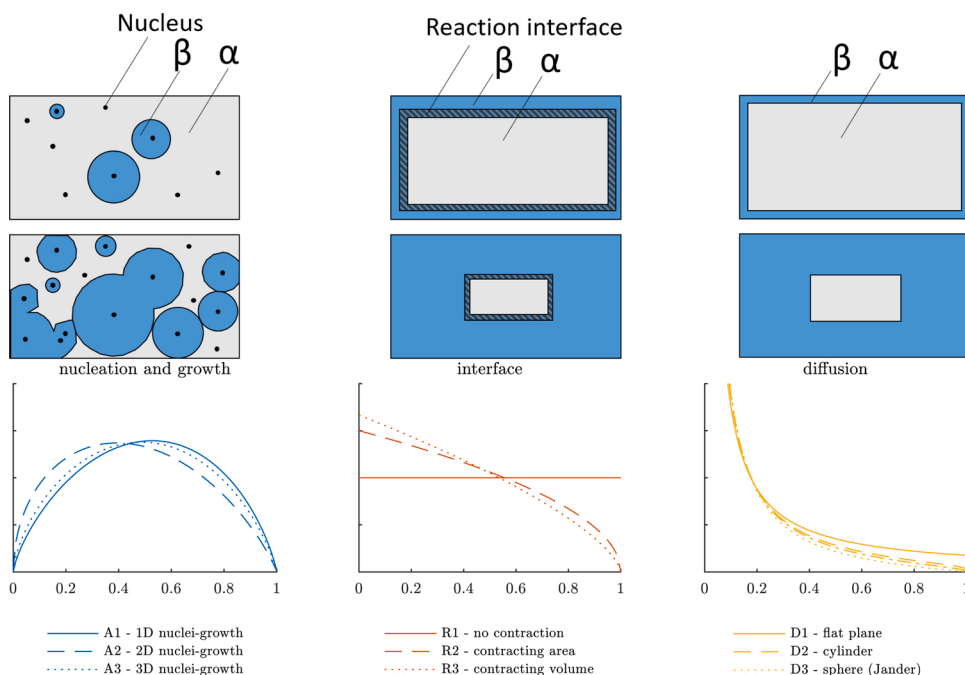


Fig. 5. Reaction models relevant to this work. The cartoons show a schematic illustration of the start and end situation of a primary crystallite, with α the reactant phase and β the product phase. The diagrams show typical shapes of isothermal isobaric reaction trajectories where left: nucleation and growth rate is limiting, middle: The advancement of the reaction interface is rate limiting, right: diffusion through the product layer is rate limiting. The reaction model codings A(1–3), R(1–3) and D(1–4) [25] are used in this work.

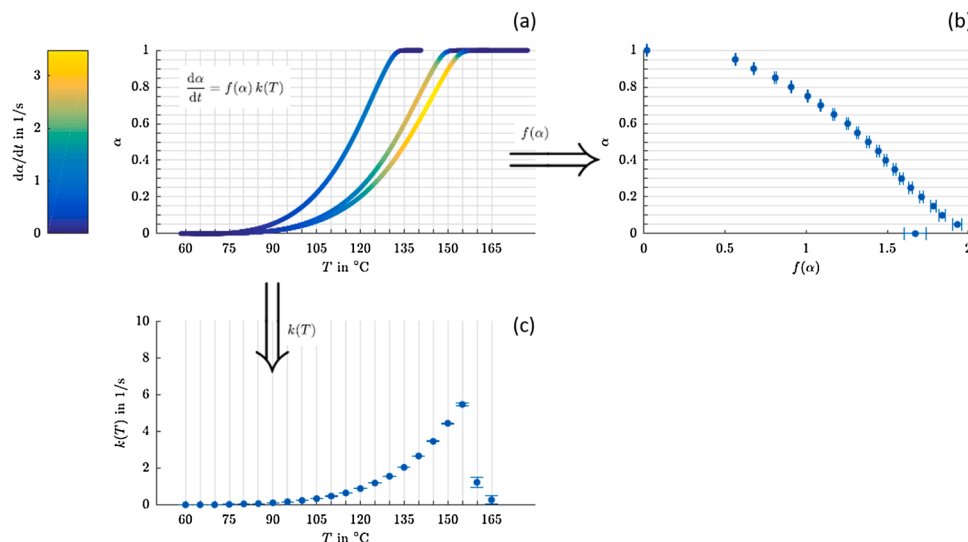


Fig. 6. Illustration of the tensor NPK method. Experimental data (a) is separated into the contributions of the independent variables conversion dependency $f(\alpha)$ (b) and temperature dependency $k(T)$ (c).

c [–] a constant [17]. At $p_f = p_{eq}$, there is virtually no nucleation. When the vapour pressure of the film approaches the critical pressure p^* , the nucleation rate increases drastically. That means, when $p_f = p^*$, hydrate formation rapidly increases as nucleation is no longer inhibiting the process.

Combining the rate of water adsorption $J_{(1)}$ and the rate of water incorporation $J_{(2)}$, the actual conversion rate J is drawn in Fig. 4c. The intersections between the two rates $J_{(1)}$ and $J_{(2)}$ indicate the actual conversion rate J as a function of p_f . It is visible that inside the MZ, the conversion rate J is limited by the nucleation rate, $J_{(2)}$. Outside the MZ, the conversion rate is limited by the adsorption rate, $J_{(1)}$. As can be seen in Fig. 4c, the vapour pressure of the film p_f stabilises at p^* outside the metastable zone ($p > p^*$), because of the drastic increase of the nucleation rate at the critical pressure p^* . The rate of hydration outside the metastable zone is therefore

$$J_{(1)} = \frac{D}{dRT}(p - p^*) \quad (9)$$

4. Non-parametric kinetic analysis

4.1. Relevant kinetic models

A nucleation limitation typically influences the conversion dependency of a reaction. With the goal to differentiate between the possible reaction progresses we consider three fundamentally different models which determine the conversion dependency. Typical shapes have been derived for nucleation, (A), reaction interface (R) and diffusion through the product layer (D) (see [25] for an extensive review). By comparing the experimental conversion dependency with the theoretically derived reaction models, we are able to evaluate our hypothesis of nucleation and vapour diffusion limitation.

In case of (A), a nucleation and growth limited process (Fig. 5, left), the initial conversion rate is slow due to the time required for a significant number of nuclei of the new phase β to form and begin growing. During the intermediate period the transformation is rapid as the nuclei grow into particles and consume the old phase while nuclei continue to form in the remaining parent phase. Once the transformation is almost complete, there remains little α phase material for further nucleation and the production of β particles begins to slow. Additionally, the β phase particles begin to touch one another, forming a boundary where growth stops. Avrami-like equations are used to demonstrate the presence/absence of accelerating kinetics due to nucleation-growth

phenomena, coded as A1, A2 and A3 respectively [26,27].

For (R), a reaction interface limitation (Fig. 5, middle), the initial conversion rate is high, because there is initially maximum interface to react. When the interface contracts due to inwards advancement of the reaction interface, less surface is available to react and the production of new β phase slows down. The different models according to this scenario are coded as R1, R2 and R3.

When (D), diffusion through the product layer is rate-limiting (Fig. 5, right), the initial conversion rate is high, because there is initially no product layer, which forms a barrier for diffusion of reactants. The conversion rate rapidly decreases with the build-up of product and typically stagnates when the transformation is almost complete, because a thick product layer inhibits the supply of reactants. The different models according to this scenario are coded D1, D2, D3 and D4. It should be noted that this model holds for diffusion of the reactants (water), through the solid product, not for diffusion of water through the atmosphere.

4.2. Algorithm

In order to compare our two-step hydration hypothesis with known kinetic models, we made use of non-parametric kinetic analysis as described by Birkelbach et al. [28]

Due to the complexity of gas-solid reactions, it is not practical, if even possible, to model all the individual processes taking place during the reaction. Issues range from collecting sufficient data, distinguishing the effects in experimental data to finding the right models for each process. As a solution, we use the common simplification to the single step approximation. It is applicable, when one of the processes is significantly slower than all the other ones. Then this process determines the overall rate of the reaction and it is referred to as the rate limiting step.

The single step approximation formula for gas-solid reactions is essentially a synthesis of solid-state and homogeneous reaction rate models:

$$\frac{d\alpha}{dt} = f(\alpha)k(T)h(p) \quad (10)$$

This rate formula is usually referred to as the general kinetic equation [29], where $f(\alpha)$ is the effect of the advancement of the reaction front in the solid as a function of the conversion α , often referred to as reaction model (Section 4.1). $k(T)$, is the effect of the absolute temperature and $h(p)$ is the driving force term as a function of the partial vapour pressure p

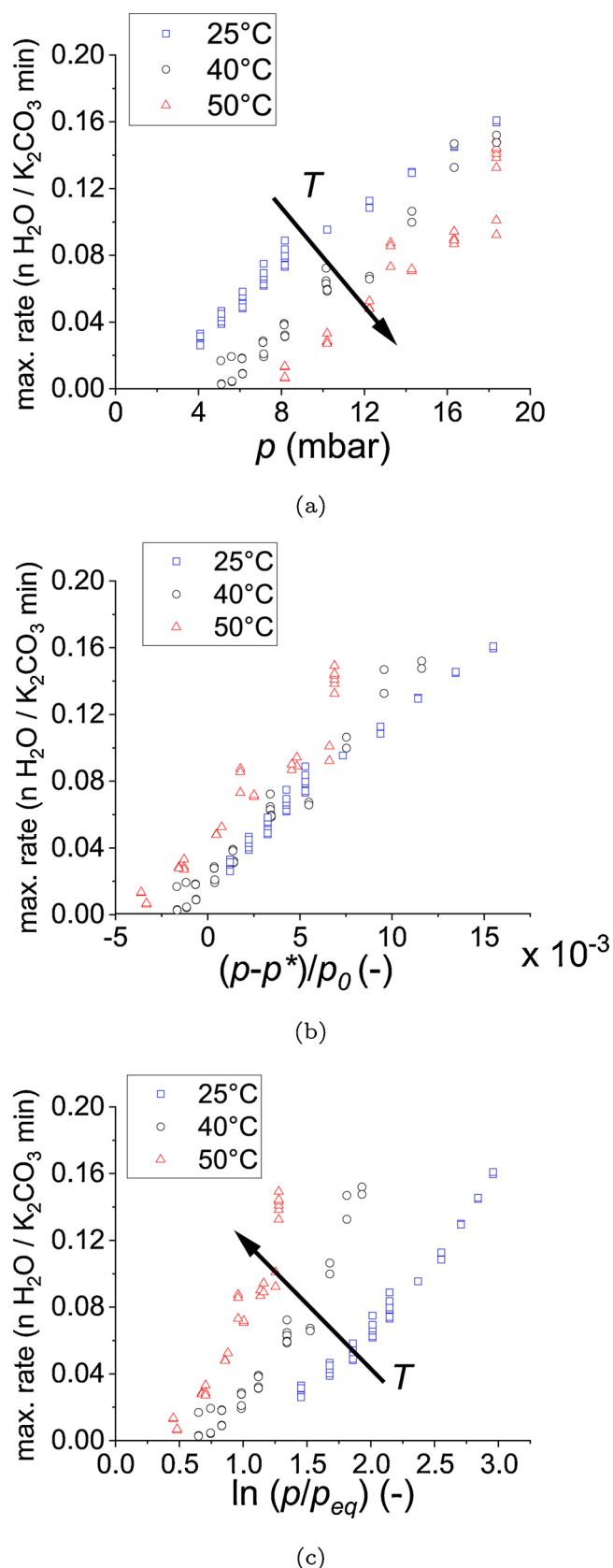


Fig. 7. Pressure dependencies of the maximum hydration rate in isothermal-isobaric experiments. The maximum rate is plotted against (a) the partial water vapour pressure p , (b) the diffusion driving force $(p - p^*)/p_0$ and (c) the chemical driving force $\ln p/p_{eq}$.

[Pa].

The temperature dependency $k(T)$ is usually expressed by the Arrhenius equation,

$$k(T) = A \exp(-E_a/RT) \quad (11)$$

with A [s^{-1}] the pre-exponential factor and E_a [J/mol] the apparent activation energy.

Various variants for the driving force term $h(p)$ have been proposed [30–32]. For non-parametric modelling, only an expression for the driving force of the rate-limiting step is required. In accordance with our theoretical considerations in Section 4.1, we chose two characteristic driving forces: in case the chemical reaction is rate limiting, we use the unitless thermodynamic driving force of the reaction ΔG

$$h(p, p_{eq}) = h(\Delta G) \propto h\left(\ln \frac{p}{p_{eq}}\right). \quad (12)$$

Since this equation is based on the assumption, that essentially a chemical reaction is limiting the overall rate, the equation will be referred to as the chemical driving force.

In case the diffusion through the gas bulk is rate limiting, we use Eq. (13) in analogy to Fick's law in Eq. (9)

$$h(p, p_f) = h\left(\frac{p - p^*}{p^0}\right) \quad (13)$$

with p^0 as an arbitrary reference pressure (here, we use the IUPAC standard pressure 10⁵Pa). Here we used the critical pressure p^* as the vapour pressure of the film (see Eq. (9)). This equation will be referred to as the diffusion driving force.

The tensor NPK method [20] which we use in this work, separates the effect of the conversion, temperature and pressure on the reaction rate based on the General Kinetic Equation. It is model-free, in the sense that no assumption about the functional form of any effect is made beforehand. Only the characteristic variables for each effect, i.e. conversion, temperature and a driving force, are required. The shape of the functions f , k and h is then determined from the experimental data with a data-driven algorithm. Fig. 6 displays an illustration of the tensor NPK method, a typical conversion dependency plot (Fig. 6b) and temperature dependency plot (Fig. 6c) is shown.

5. Results and discussion

5.1. Conversion and temperature dependency

Hydration rates were obtained at constant driving force by performing experiments in isobaric, isothermal conditions. Rates were measured below and above the metastable zone boundary with $p - p^*$ between -5 and $+15$ mbar. The maximum hydration rate in isothermal-isobaric conditions is plotted as a function of vapour pressure p (Fig. 7a). Here it is visible that the rate increases monotonically with the vapour pressure. A linear relation between pressure and rate is observed, especially at vapour pressures below 12 mbar. The rate is generally higher at lower temperatures. When the rate is plotted as a function of the diffusion driving force (Fig. 7b), the linearity remains, but no clear temperature dependency is visible. When the dataset is plotted against the chemical driving force (Fig. 7c), an exponential relation between rate and driving force is recognised, the rate is generally higher at higher temperatures.

The data were further analysed with the tensor NPK method. We will focus here on the conversion and temperature dependency. The vapour pressure dependency of the rate based on NPK analysis using the Data in Brief. The vapour pressure dependency found in NPK analyses is in line with the observations in Fig. 7.

The chemical driving force (Eq. (12)) was used first for NPK analysis.

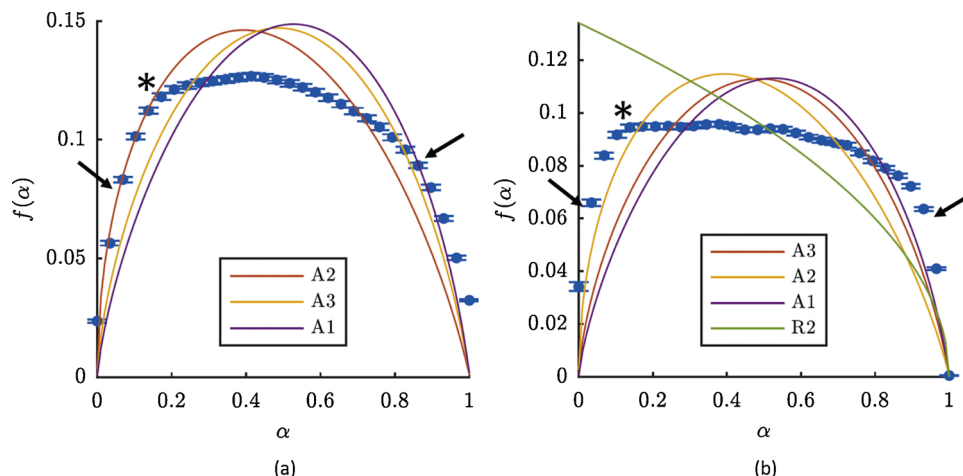


Fig. 8. Conversion dependency of the hydration reaction of K_2CO_3 according to the chemical driving force. (a) Isobaric isothermal conditions, (b) isobaric (non-isothermal) conditions. Features of nucleation-growth phenomena (arrows) and a reaction interface (*) are visible.

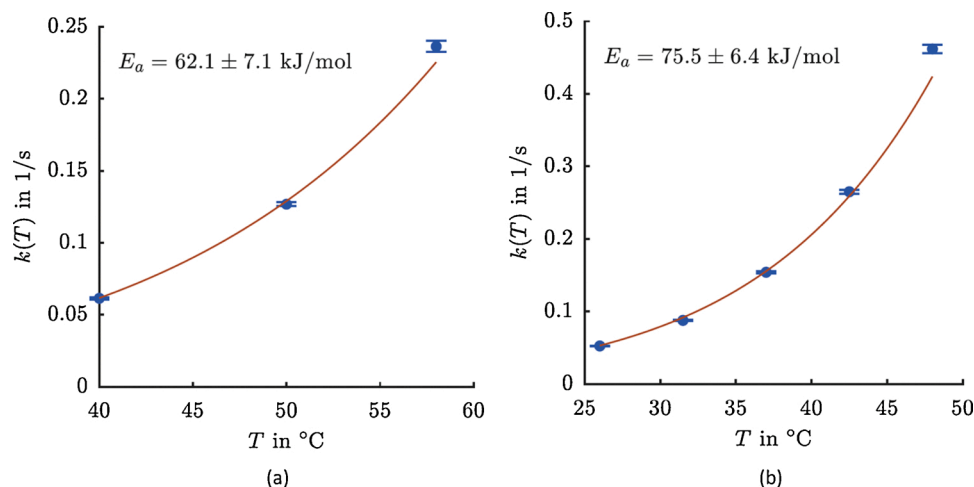


Fig. 9. Temperature dependency of the hydration reaction of K_2CO_3 according to the chemical driving force. (a) Isobaric isothermal conditions, (b) isobaric (non-isothermal) conditions.

Table 1

Hydration enthalpies of the considered salts and apparent activation energies identified in this work. The hydration enthalpies are calculated from p , T data published in a previous study [17] using the basic thermodynamic equation for equilibrium between a condensed phase (solid or liquid) and the vapour phase of a pure substance, under conditions of low pressure [33].

Salt	ΔH^0 (kJ/mol water)	E_a (kJ/mol water)
K_2CO_3 (isothermal, isobaric)	63.4	65.6 ± 18.2
		67.4 ± 10.5
		62.1 ± 7.1
K_2CO_3 (isobaric)		75.5 ± 6.4
$CuCl_2$ (isobaric)	61.4	79.1 ± 10.2
$LiCl$ (isobaric)	58.2	52.9 ± 4.3
$MgCl_2 \cdot 4H_2O$ (isobaric)	56.9	52.1 ± 7.8

The conversion dependency (Fig. 8a) shows typical features of accelerating kinetics due to nucleation phenomena. However, it also shows a plateau(*) at medium conversion, which is rather a characteristic of a reaction interface. In order to have a comprehensive view on the conversion dependency, the experiment was repeated under isobaric, non-isothermal conditions. For experimental details of the isobaric experiment we refer to the Data in Brief. We found that the isobaric experiment agrees well with the isobaric-isothermal experiment (Fig. 8b). In both

experimental conditions, the conversion dependency shows features of nucleation-growth phenomena (indicated by the arrow) and an anomalous plateau (*), which indicates a steady reaction front. It should be noted that diffusion through the product layer is ruled out as reaction model on the basis of this analysis, since the experimental conversion dependency does not match this model.

The underlying assumption of the chemical driving force is that the rate limiting step is a chemical reaction with a single and constant energy barrier. Consequently, the temperature dependency, shown in Fig. 9, is interpreted in terms of the Arrhenius equation (11). The identified temperature dependency is well described by the equation and the apparent activation energy is 62.1 ± 7.1 kJ/mol for the isobaric-isothermal experiment and 75.5 ± 6.4 kJ/mol for the isobaric experiment. The identified apparent activation energies of various salts are gathered in Table 1, for experimental details we refer to the Data in Brief. It is interesting that the value of the apparent activation energy is in most of the cases similar to the hydration enthalpy.

Using the same dataset, a kinetic model with the diffusion driving force (Eq. (13)) was derived. The conversion dependency (Fig. 10) is once again identified as showing features of both nucleation-growth phenomena (indicated by arrows) and a steady reaction front (indicated by the asterisk). Like in the first analysis, diffusion through the product layer is ruled out as reaction model, since the experimental

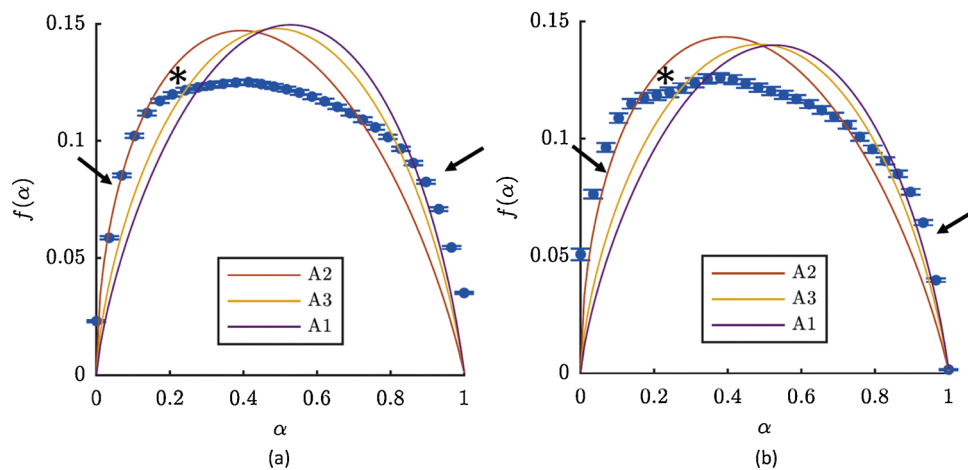


Fig. 10. Conversion dependency of the hydration reaction of K_2CO_3 according to the diffusion driving force. (a) Isobaric isothermal conditions, (b) isobaric (non-isothermal) conditions. Features of nucleation-growth phenomena (arrows) and a reaction interface (*) are visible.

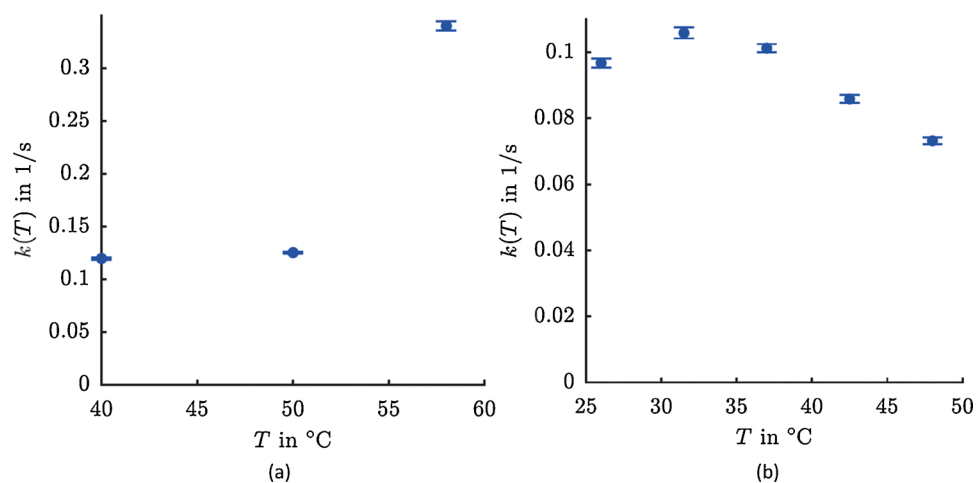


Fig. 11. Temperature dependency of the hydration reaction of K_2CO_3 according to the diffusion driving force. (a) Isobaric isothermal conditions, (b) isobaric (non-isothermal) conditions.

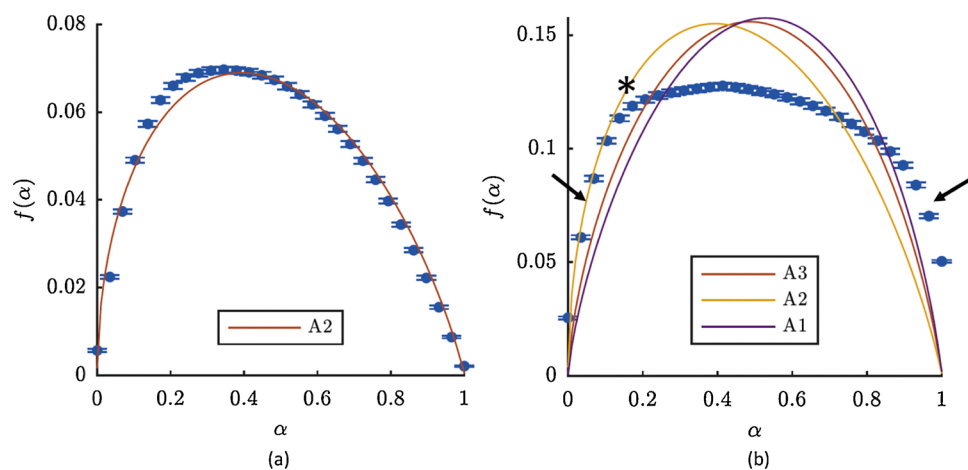


Fig. 12. Conversion dependency of the hydration reaction of K_2CO_3 (a) according to the chemical driving force inside the metastable zone – accelerating kinetics due to nucleation-growth phenomena is visible. (b) According to the diffusion driving force outside the metastable zone – features of nucleation-growth phenomena (arrows) and a reaction interface (*) are visible. Isobaric isothermal conditions.

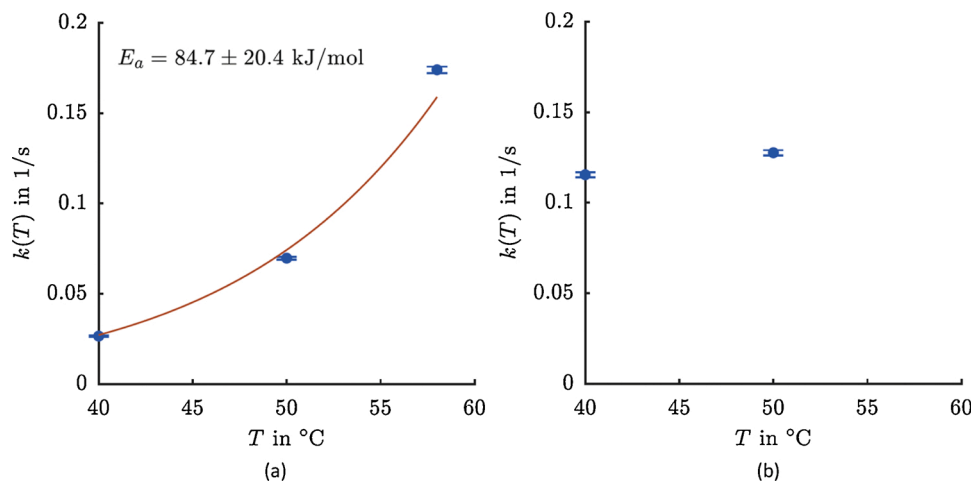


Fig. 13. Temperature dependency of the hydration reaction of K_2CO_3 (a) according to the chemical driving force inside the metastable zone, (b) according to the diffusion driving force outside the metastable zone. Isobaric isothermal conditions.

conversion dependency does not match this model.

The temperature dependency in the case of the diffusion driving force has a clear difference with respect to the chemical driving force. There is no temperature dependency which can be interpreted in terms of the Arrhenius equation (Fig. 11). As expected, a description based on diffusion limitation mainly depends on the pressure difference and hardly on the temperature.

Lastly, for separate analysis of the hydration rate in the metastable zone, the isothermal-isobaric dataset was split into data inside the MZ and data outside the MZ. The chemical driving force is used to model the data in the MZ, the diffusion driving force is used to model the data outside the MZ, in line with the two-step hypothesis; the resulting models are shown in Figs. 12 and 13.

Inside the metastable zone (Fig. 12a), the conversion dependency shows no clear limitation due to a reaction interface, the conversion dependency is well fitted with the mathematics. The apparent activation energy is 84.7 ± 20.4 kJ/mol (Fig. 13a).

Outside the metastable zone (Fig. 12b), the plateau (*) in the conversion dependency indicates that a constant reaction interface (a non-contracting phase boundary) is involved. The rate does not depend on the reaction coordinate anymore after circa 15% conversion. That points towards a limitation other than nucleation. Comparison with the basic conversion dependencies (Fig. 5) shows that other processes such as the continuous advancement of a reaction front or build-up of a product layer are not limiting either. This is in agreement with the view that water diffusion to the wetting layer is the limiting process at high supersaturations. Furthermore, migration of the solid is expected during the crystallisation, introducing air-solid surface area while the reaction proceeds [34].

A model involving surface and phase-boundary controlled reactions was originally formulated by Mampel [35], recently reconstructed [36] as nucleation and anisotropic growth model, and the differential kinetic equations for this type of consecutive reactions have been derived by Ogasawara and Koga for dehydration [37]. The use of Mampel's model in isothermal and isobaric conditions [38,39] for hydration offers therefore an interesting field for further study.

5.2. Link between the chemical and the diffusion driving force

Reconsidering the outcome of the NPK analysis: Why does the chemical driving force $\ln p/p_{eq}$ lead to a consistent model with clear activation energies (Figs. 9 versus 11), when diffusion should be the rate limiting step outside the MZ? Only one step can be rate limiting at a time. As it turns out, the Arrhenius like temperature dependency is simply an artefact of the reaction equilibrium. Consequently, the

apparent activation energy in that analysis must not be interpreted in terms of a classical energy barrier.

It can be shown that there is a link between the chemical and the diffusion driving force. By rearranging the General Kinetic Equation with the diffusion driving force in Eq. (13), one arrives at a similar functional form as the classic kinetic equation with the chemical driving force in Eq. (12):

$$\frac{d\alpha}{dt} = f(\alpha) C \frac{p - p^*}{p^0} = f(\alpha) C \frac{p_{eq}}{p^0} \left[\frac{p}{p_{eq}} - \frac{p^*}{p_{eq}} \right] \quad (14)$$

where C [-] is a constant. When we make use of Eq. (4) to substitute $\frac{p_{eq}}{p^0}$, the term in square brackets is aggregated as $h(p, p_{eq})$

$$\frac{d\alpha}{dt} = f(\alpha) C \exp\left(\frac{\Delta S^0}{R}\right) \exp\left(-\frac{\Delta H^0}{RT}\right) h(p, p_{eq}) \quad (15)$$

Comparing the result with the Arrhenius rate equation (11), one discovers the similarity:

$$\frac{d\alpha}{dt} = f(\alpha) A \exp\left(-\frac{E_a}{RT}\right) h(p, p_{eq}) \quad (16)$$

In other words, if the rate limiting step is diffusion to the wetting layer and the classical kinetic model in Eq. (16) is used to model the kinetics, one will still find an Arrhenius-like temperature dependency. Only, the apparent activation energy would not be related to the energy barrier, but simply to the enthalpy of the reaction, that is, $E_a \rightarrow \Delta H^0$. A typical example of this artefact can be seen in [40].

6. Conclusion

In this work, we hypothesised a generic mechanism for hydration, which includes two steps: (1) water adsorption and ion dissolution (a wetting film on the salt), and (2) hydrate crystallisation. The two steps are assumed to be in momentary balance during the hydration process. Based on this, nucleation is rate limiting at low supersaturations of water vapour (inside the metastable zone) and diffusion to the wetting layer is rate limiting at high supersaturations (outside the metastable zone). We have seen that the vapour pressure of the wetting film of the salt crystal stabilises at the metastable zone boundary p^* . The driving force for hydration outside the metastable zone is then the pressure difference between the atmospheric vapour pressure and the vapour pressure of the wetting film, $p - p^*$.

The two-step hypothesis is supported by the results of a kinetic analysis with the Tensor NPK method. Three basic models were

considered to fit the conversion dependency: nucleation, a reaction interface and diffusion through the product. The vapour pressure dependency was considered in two different ways: as a chemical driving force, which assumes that the chemical reaction is rate limiting and as a diffusion driving force, which assumes that diffusion of vapour to the reacting surface is rate limiting.

NPK analysis of K_2CO_3 indicates that nucleation plays a central role inside the metastable zone (at low supersaturations) as expected. Outside the metastable zone (at high supersaturations) the reaction rate is constant and irrespective of the reaction coordinate after circa 15% conversion. That points towards a limitation other than nucleation. The analysis shows that other processes such as the continuous advancement of a reaction front or build-up of a product layer are not limiting either. These results agree with the concept of water diffusion to the surface wetting layer as limiting process at high supersaturations.

Interestingly, the kinetics of hydration can be modelled both with the chemical and the diffusion driving force. It could be shown, that even if diffusion is rate limiting (outside the metastable zone), an Arrhenius like temperature dependency can be observed. In this case the apparent activation energy is equal to the hydration enthalpy per mole water and must not be interpreted as an energy barrier – it is an artefact of the reaction equilibrium.

Author contributions

Leyla-Cann Sögütöglu: Conceptualization, methodology, formal analysis, investigation, resources, writing – original draft, visualisation, data curation, project administration. Felix Birkelbach: Conceptualization, methodology, software, validation, formal analysis, resources, writing – original draft, visualisation, data curation, project administration. Andreas Werner: Supervision, funding acquisition. Hartmut Fischer: Conceptualization, methodology, writing – review & editing. Henk Huinink: Conceptualization, methodology, supervision, writing – review & editing, visualization, data curation, project administration. Olaf Adan: Writing – review & editing, funding acquisition.

Declaration of Competing Interest

The authors report no declarations of interest.

Acknowledgements

Part of this project has received funding from the European Unions Horizon 2020 Research and Innovation Programme under grant agreement no. 680450. This work reflects only the author's view. The European Commission is not responsible for any use that may be made of this information.

The authors would like to thank the Austrian Research Promotion Agency (FFG) for their financial support of the project SolidHeat Pressure (#853593) and Hans Dalderop for his technical support.

Appendix A. Supplementary data

Supplementary data associated with this article can be found, in the online version, at <https://doi.org/10.1016/j.tca.2020.178819>.

References

- [1] L. Scapino, H.A. Zondag, J. Van Bael, J. Diriken, C.C. Rindt, Sorption heat storage for long-term low-temperature applications: a review on the advancements at material and prototype scale, *Appl. Energy* 190 (2017) 920–948.
- [2] B. Michel, P. Neveu, N. Mazet, Comparison of closed and open thermochemical processes, for long-term thermal energy storage applications, *Energy* 72 (2014) 702–716.
- [3] P.A.J. Donkers, L.C. Sögütöglu, H.P. Huinink, H.R. Fischer, O.C.G. Adan, A review of salt hydrates for seasonal heat storage in domestic applications, *Appl. Energy* 199 (2017) 45–68, <https://doi.org/10.1016/j.apenergy.2017.04.080>.
- [4] P.A.J. Donkers, S. Beckert, L. Pel, F. Stallmach, M. Steiger, O.C.G. Adan, Water transport in $MgSO_4 \cdot 7H_2O$ during dehydration in view of thermal storage, *J. Phys. Chem. C* 119 (52) (2015) 28711–28720, <https://doi.org/10.1021/acs.jpcc.5b08730>.
- [5] K. Posern, C. Kaps, Calorimetric studies of thermochemical heat storage materials based on mixtures of $MgSO_4$ and $MgCl_2$, *Thermochim. Acta* 502 (1–2) (2010) 73–76.
- [6] V. Van Essen, H. Zondag, J.C. Gores, L. Bleijendaal, M. Bakker, R. Schuitema, W. Van Helden, Z. He, C. Rindt, Characterization of $MgSO_4$ hydrate for thermochemical seasonal heat storage, *J. Sol. Energy Eng.* 131 (4) (2009) 041014.
- [7] L.C. Sögütöglu, P.A.J. Donkers, H.R. Fischer, H.P. Huinink, O.C.G. Adan, In-depth investigation of thermochemical performance in a heat battery: cyclic analysis of K_2CO_3 , $MgCl_2$ and Na_2S , *Appl. Energy* 215 (2018) 159–173.
- [8] M. Molenda, J. Stengler, M. Linder, A. Wörner, Reversible hydration behavior of $CaCl_2$ at high H_2O partial pressures for thermochemical energy storage, *Thermochim. Acta* 560 (2013) 76–81.
- [9] H.U. Rammelberg, T. Schmidt, W. Ruck, Hydration and dehydration of salt hydrates and hydroxides for thermal energy storage – kinetics and energy release, *Energy Procedia* 30 (2012) 362–369, <https://doi.org/10.1016/j.egypro.2012.11.043>.
- [10] C. Ferchaud, H. Zondag, J. Veldhuis, R. De Boer, Study of the reversible water vapour sorption process of $MgSO_4 \cdot 7H_2O$ and $MgCl_2 \cdot 6H_2O$ under the conditions of seasonal solar heat storage, *J. Phys. Conf. Ser.* 395 (2012) 012069.
- [11] H. Zondag, V. Van Essen, L. Bleijendaal, B. Kikkert, M. Bakker, Application of $MgCl_2 \cdot 6H_2O$ for thermochemical seasonal solar heat storage, 5th International Renewable Energy Storage Conference IRES (2010) 22–24.
- [12] E. Brunberg, The Tepidus system for seasonal heat storage and for cooling, *Thermochem. Energy Storage* 1980 (1980) 247–260.
- [13] R. De Boer, W. Haije, J. Veldhuis, S. Smeding, Solid-sorption cooling with integrated thermal storage—the sweat prototype, in: *Int. Conf. Heat Powered Cycles*, Larnaca, Cyprus, August 2004, 2004.
- [14] R. Cuypers, A. De Jong, J. Eversdijk, J. van't Spijker, H. Oversloot, B. Ingenhut, R. Cremers, N. Papen-Butterhuis, Microencapsulation of salts for enhanced thermochemical storage materials, in: 40th Annual Meeting and Exposition of the Controlled Release Society, Honolulu, Hawaii, USA, July 21–24, 2013, 2013, pp. 1–2.
- [15] Y.I. Aristov, G. Di Marco, M.M. Tokarev, V.N. Parmon, Selective water sorbents for multiple applications, 3. $CaCl_2$ solution confined in micro- and mesoporous silica gels: Pore size effect on the “solidification-melting” diagram, *React. Kinet. Catal. Lett.* 61 (1) (1997) 147–154, <https://doi.org/10.1007/BF02477527>.
- [16] M. Stanish, D. Perlmutter, Kinetics of hydration-dehydration reactions considered as solid transformations, *AIChE J.* 30 (4) (1984) 557–563.
- [17] L.-C. Sögütöglu, M. Steiger, J. Houben, D. Biemans, H.R. Fischer, P. Donkers, H. Huinink, O.C. Adan, Understanding the hydration process of salts: the impact of a nucleation barrier, *Cryst. Growth Des.* 19 (4) (2019) 2279–2288.
- [18] M. Steiger, K. Linnow, H. Juling, G. Gülker, A.E. Jarad, S. Brüggerhoff, D. Kirchner, Hydration of $MgSO_4 \cdot H_2O$ and generation of stress in porous materials, *Cryst. Growth Des.* 8 (1) (2007) 336–343.
- [19] K. Linnow, M. Niermann, D. Bonatz, K. Posern, M. Steiger, Experimental studies of the mechanism and kinetics of hydration reactions, *Energy Procedia* 48 (2014) 394–404.
- [20] F. Birkelbach, M. Deutsch, S. Flegkas, F. Winter, A. Werner, NPK 2.0: introducing tensor decompositions to the kinetic analysis of gas-solid reactions, *Int. J. Chem. Kinet.* 51 (4) (2019) 280–290, <https://doi.org/10.1002/kin.21251>.
- [21] L. Greenspan, Humidity fixed points of binary saturated aqueous solutions, *J. Res. Natl. Bur. Stand.* 81 (1) (1977) 89–96.
- [22] P. Gabbott, Principles and Applications of Thermal Analysis, John Wiley & Sons, 2008.
- [23] G.E. Ewing, H_2O on NaCl: from single molecule, to clusters, to monolayer, to thin film, to deliquescence, Intermolecular Forces and Clusters II (2005) 1–25.
- [24] S. Jennings, The mean free path in air, *J. Aerosol Sci.* 19 (2) (1988) 159–166.
- [25] A. Khawam, D.R. Flanagan, Solid-state kinetic models: basics and mathematical fundamentals, *J. Phys. Chem. B* 110 (35) (2006) 17315–17328, <https://doi.org/10.1021/jp062746a>.
- [26] M. Avrami, Kinetics of phase change. I. General theory, *J. Chem. Phys.* 7 (12) (1939) 1103–1112.
- [27] M. Avrami, Kinetics of phase change. II. Transformation-time relations for random distribution of nuclei, *J. Chem. Phys.* 8 (2) (1940) 212–224.
- [28] F. Birkelbach, M. Deutsch, A. Werner, The effect of the reaction equilibrium on the kinetics of gas-solid reactions—a non-parametric modeling study, *Renew. Energy* 152 (2020) 300–307, <https://doi.org/10.1016/j.renene.2020.01.0331>.
- [29] S. Vyazovkin, A.K. Burnham, J.M. Criado, L.A. Pérez-Maqueda, C. Popescu, N. Sbirrazzuoli, ICTAC Kinetics Committee recommendations for performing kinetic computations on thermal analysis data, *Thermochim. Acta* 520 (2011) 1–19, <https://doi.org/10.1016/j.tca.2011.03.034>.
- [30] N. Koga, L. Favregeon, S. Kodani, Impact of atmospheric water vapor on the thermal decomposition of calcium hydroxide: a universal kinetic approach to a physico-geometrical consecutive reaction in solid-gas systems under different partial pressures of product gas, *Phys. Chem. Chem. Phys.* 21 (22) (2019) 11615–11632.
- [31] M. Fukuda, L. Favregeon, N. Koga, Universal kinetic description for thermal decomposition of copper (II) hydroxide over different water vapor pressures, *J. Phys. Chem. C* 123 (34) (2019) 20903–20915.
- [32] Y. Yamamoto, L. Favregeon, N. Koga, Thermal dehydration of lithium sulfate monohydrate revisited with universal kinetic description over different temperatures and atmospheric water vapor pressures, *J. Phys. Chem. C* (2020).

- [33] L. Glasser, H.D.B. Jenkins, The thermodynamic solvate difference rule: solvation parameters and their use in interpretation of the role of bound solvent in condensed-phase solvates, *Inorg. Chem.* 46 (23) (2007) 9768–9778.
- [34] W.J. van Enkevort, J.H. Los, On the creeping of saturated salt solutions, *Cryst. Growth Des.* 13 (5) (2013) 1838–1848.
- [35] K. Mampel, Time conversion formulas for heterogeneous reactions at the phase boundaries of solid bodies. I. The development of the mathematical method and the derivation of area conversion formulas, *Z. Phys. Chem. Abt. A* 187 (1940) 43–57.
- [36] L. Favergeon, M. Pijolat, M. Soustelle, Surface nucleation and anisotropic growth models for solid-state reactions, *Thermochim. Acta* 654 (2017) 18–27.
- [37] H. Ogasawara, N. Koga, Kinetic modeling for thermal dehydration of ferrous oxalate dihydrate polymorphs: a combined model for induction period-surface reaction-phase boundary reaction, *J. Phys. Chem. A* 118 (13) (2014) 2401–2412.
- [38] H. Galai, F. Valdivieso, M. Pijolat, M. Trabelsi-Ayadi, Kinetic study of a $\text{HGdP}_2\text{O}_7 \cdot 3\text{H}_2\text{O}$ dehydration step, *Thermochim. Acta* 428 (1–2) (2005) 105–111.
- [39] V. Bouineau, M. Pijolat, M. Soustelle, Characterisation of the chemical reactivity of a CaCO_3 powder for its decomposition, *J. Eur. Ceram.* 18 (9) (1998) 1319–1324.
- [40] M. Gaeini, S. Shaik, C. Rindt, Characterization of potassium carbonate salt hydrate for thermochemical energy storage in buildings, *Energy Build.* 196 (2019) 178–193.